Leino, Mikko K.; Ala-Laurinaho, Juha; Purisha, Zenith; Särkkä, Simo; Viikari, Ville

Millimeter-wave imaging method based on frequency-diverse subarrays

Published in:
GSMM 2019 - 12th Global Symposium on Millimeter Waves, Proceeding

DOI:
10.1109/GSMM.2019.8797670

Published: 01/05/2019

Document Version
Peer-reviewed accepted author manuscript, also known as Final accepted manuscript or Post-print

Please cite the original version:
Leino, M. K., Ala-Laurinaho, J., Purisha, Z., Särkkä, S., & Viikari, V. (2019). Millimeter-wave imaging method based on frequency-diverse subarrays. In *GSMM 2019 - 12th Global Symposium on Millimeter Waves, Proceeding* (pp. 84-86). Article 8797670 IEEE. https://doi.org/10.1109/GSMM.2019.8797670

Millimeter-wave Imaging Method based on Frequency-Diverse Subarrays

Mikko K. Leino[1], Juha Ala-Laurinaho[1], Zenith Purisha[2], Simo Särkkä[2], and Ville Viikari[1]
[1]*Department of Electronics and Nanoengineering,* [2]*Department of Electrical Engineering and Automation*
Aalto University School of Electrical Engineering
Espoo, Finland
mikko.k.leino@aalto.fi, juha.ala-laurinaho@aalto.fi, zenith.purisha@aalto.fi, simo.sarkka@aalto.fi, and ville.viikari@aalto.fi

***Abstract*—Method to reconstruct images with frequency diverse subarrays at millimeter-wave frequencies is presented. The imaging system consists of a set of transmit and receive subarrays each having unique, strongly frequency-dependent radiation pattern. Signal transmissions between different transmit and receive subarray pairs are recorded at multitude of frequencies and the image is solved from the set of these measurements. Target space is observed with each subarray pair and with the known subarray field patterns, the target locations are determined. Simulation study of the method has been conducted and the evaluation of the results proves that the method is viable and could be used for imaging purposes.**

***Index Terms*—millimeter-wave imaging, frequency-diverse antenna, subarrays**

I. Introduction

Electrical beam steering is superseding traditionally used mechanical beam steering in many radar applications. Electrical beam steering is realized with antenna arrays, whose element phasing can be adjusted to obtain beams radiating to different directions. Element phasing can be realized either with adjustable phase shifters, or with traveling wave antennas, whose beam inherently steers with the carrier frequency. The approach based on adjustable phase shifters offers the best control of the beam but leads to complex and costly hardware especially in case of large arrays [1]–[3]. The solutions where the beam steers with the carrier frequency are simpler in hardware, but imposes other challenges [4]–[6]. First, the beam can be easily steered only in one plane only, severely limiting the angular range. Second, the bandwidth, which is needed to achieve distance resolution, is partly sacrificed to achieve angular resolution.

A method utilizing frequency-diverse antenna patterns in millimeter-wave imaging has been previously studied [7], [8]. This makes it possible to simplify the hardware significantly, while maintaining the needed distance and angular resolution. Similarly to MIMO radars as in [9], the method utilizes diversity offered by the multiple probing signals but with simple signal processing. Demonstrations of the method have been realized using meta-surfaces or reverberating multi-mode resonators [7], [8]. In this paper, we present an alternative array configuration that is more straightforward to design and manufacture.

This work was supported in part by Saab AB.

II. Estimation Problem Formulation

The conceptual figure of the problem setup is presented in Fig. 1. The imaging system consists of many transmit and receive subarrays each having different, strongly frequency-dependent radiation pattern. Each subarray radiates, according to its unique pattern, its own field, which is then reflected back from N targets. The reflected signal is received by every subarray according to the subarray patterns.

The observed responses provide frequency-dependent observation data $y_{mn}(f)$ for each TX-RX pair, with n denoting transmitting and m receiving subarray number. The signal model for the system can be formulated as:

$$y_{mn}(f) = \sum_{i=1}^{N} (\mathbf{E}_n(\theta_i, \phi_i, f) \cdot \mathbf{E}_m(\theta_i, \phi_i, f)) \Gamma_i \frac{e^{-j\frac{4\pi f r_i}{c}}}{(4\pi r_i)^2}. \quad (1)$$

The total observation is the sum of the single target responses, where an individual target i locates in angular direction of θ_i, ϕ_i with the distance of r_i from the imaging system. The reflection from the target is denoted with Γ_i. Furthermore, the scalar product of the transmitting and receiving subarray electric fields, $\mathbf{E}_n$ and $\mathbf{E}_m$ respectively, is calculated to preserve the phase information, which is essential for the distance calculation. From (1) we can evaluate the target location variables $\theta_i, \phi_i, r_i, \Gamma_i$, and N, if the radiated fields of the transmitting and receiving subarrays are known over the target space.

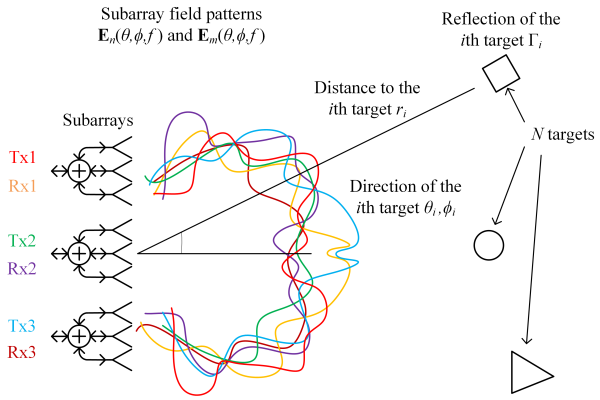

Fig. 1. Conceptual picture of the imaging problem setup.

III. Evaluation of the Imaging Method

First step with the evaluation is the discretization of the target space. The 3D target space is divided into voxels, which are identified with the spherical coordinates θ_i, ϕ_j, r_l. The angular resolution depends on the resolution of the subarray field patterns whereas the range is dependent on the observation bandwidth and the frequency step between the observations. In this study, the targets are assumed to be stationary in a single voxel and the reflections from them are perfect i.e. Γ_i for each target is assumed to be 1 in linear scale. In reality, Γ_i is affected by the radar cross section (RCS) of the target i.e. the target shape, material, and the incident angle of the illumination. However, RCS is omitted from this study to simplify the examination of the method.

$\mathbf{O}$ is the vector containing the observation data $y_{mn}(f_k)$ of the mn TX-RX subarray pair at kth frequency, as expressed in (1). It can be expressed as a product of the field data and the target data as:

$$\mathbf{O}(y_{mn}(f_k)) = \mathbf{A}(P_{mn}(\theta_i, \phi_j, f_k), r_l)\mathbf{T}(\Gamma(\theta_i, \phi_j, r_l)). \quad (2)$$

$\mathbf{T}$ is the vector containing the target data over the target space (θ_i, ϕ_j, r_l) and $\mathbf{A}$ is the matrix containing the field data $P_{mn}(\theta_i, \phi_j, f_k)$ towards the target space. $\mathbf{A}$ is constructed using the aforementioned TX-RX subarray pairs and the scalar products of their electric fields as a basis of the matrix elements:

$$P_{mn}(\theta_i, \phi_j, f_k) = \mathbf{E}_n(\theta_i, \phi_j, f_k) \cdot \mathbf{E}_m(\theta_i, \phi_j, f_k). \quad (3)$$

The matrix element for $\mathbf{A}$ is:

$$\mathbf{A}_{m,n,i,j,k,l} = P_{mn}(\theta_i, \phi_j, f_k)\frac{e^{-j\frac{4\pi f_k r_l}{c}}}{(4\pi r_l)^2}. \quad (4)$$

The elements of vectors $\mathbf{O}$ and $\mathbf{T}$ and matrix $\mathbf{A}$ are arranged so that they satisfy (2).

The image reconstruction is based on solving the matrix equation (2) for the target data as:

$$\mathbf{T} = \mathbf{A}^{+}\mathbf{O}, \quad (5)$$

where $\mathbf{A}^{+}$ is the pseudoinverse of the field data matrix. Basically, the target data vector contains the reflection information of the target space for each voxel. By solving the target data using the field and observation data, we should find the target's reflection value $\Gamma(\theta_i, \phi_j, r_l)$ in that voxel, if there is a target. By finding the voxels with reflection values, we can identify the target locations.

To validate the performance of the method with simulations, we have chosen to simplify the problem and reduced the 3D target space to 2D. This reduces calculation time but still gives a fairly good estimation of what the method is capable of. Hence, the target evaluation is chosen to cover the azimuth cut and the distance.

Evaluation is done using the simulated antenna array with 64 elements, that radiate ideal cosine patterns at 38–42 GHz frequency range. Element spacing is $\lambda/2$ at 40 GHz. The elements are divided to eight subarrays, thus we can observe

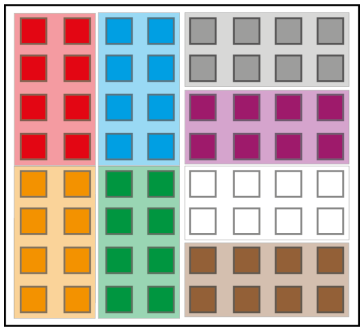

Fig. 2. Subarray shapes and locations in the 64-element antenna system.

36 independent TX-RX pairs due to the reciprocal responses. The shapes of the subarrays and their locations in the antenna system are shown in Fig. 2.

Furthermore, the variation over the frequency is required, as it benefits the angular resolution. Distinguishable radiation patterns with frequency-dependency are achieved by feeding each subarray element out-of-phase with different time-delay lines. Each subarray has an unique element-phasing scheme: an example is shown in Fig. 3 at 40 GHz. It shows the relative time-delays in wavelengths for each element compared to the reference one. The maximum time-delays used in the feeding are 2.40λ at 40 GHz. The subarrays are configured as simple 4x2 arrays as the shape of the subarrays are relatively insignificant when considering the performance of the evaluation method. In addition, the used element phasing with time-delay lines gives much more of the wanted frequency diversity between the subarray patterns than the phase difference caused by the element spacing. However, it would be beneficial to study optimal subarray configurations.

The electric field patterns of subarrays are designed so that the target space is fully illuminated, but also so that the subarrays illuminate different angular areas. Hence, a noticeable deviation in field strength between different subarrays over the angular space is achieved, which further creates diversity between the TX-RX pair responses. This is thought to increase the performance, when the individual responses are involved in the image reconstruction calculation. The azimuth cut of the normalized amplitude responses for each TX-RX pairs are shown in Fig. 4 at 40 GHz.

Angular resolution of 1° is used in the performance analysis of the method and thus the angular space is discretized to 181

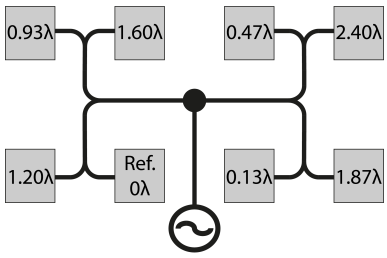

Fig. 3. Element-phasing example of one of the subarrays at 40 GHz. Note: the lengths of the lines are not in scale according to the delays.

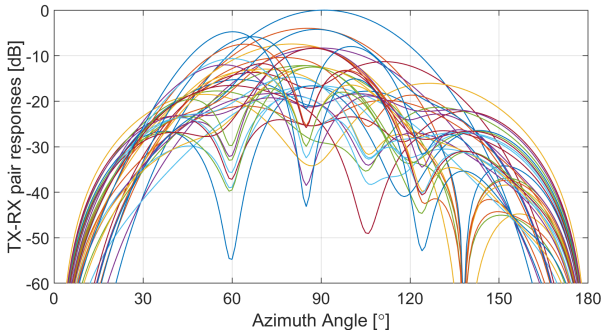

Fig. 4. Normalized TX-RX subarray pair amplitude responses at 40 GHz. Presented 36 individual responses are utilized in the evaluation method.

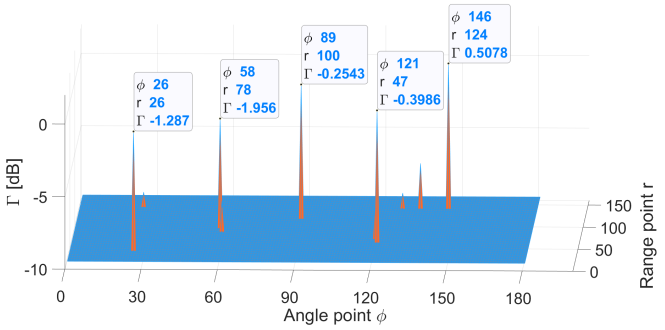

Fig. 5. The locations of five targets retrieved by the proposed method. The correct target locations in (ϕ,r) points are (30,25), (60,75), (90,100), (120,50), and (150,125).

points. However, the cosine-shaped element patterns limit the practical field-of-view to 30°– 150°. The range resolution is affected by the bandwidth and the frequency step between the observations. The maximum range is also dependent on the frequency step and after the maximum range is reached, the further targets start aliasing to the lower range. The range is discretized to 151 points with aim to see how accurately the correct target location can be identified, and how far the imaging can be done with different frequency steps. In this study, the maximum range corresponds to 0.75 m.

The primary bandwidth for observations ranges from 38 GHz to 42 GHz, with frequency step of 200 MHz. The evaluation method has been studied by placing a target in each pixel of the 2D target space. The targets can be found fairly well in the areas with high illumination and the range point after the aliasing starts has been identified.

Further simulations have been made to analyze the effect of the observation bandwidth and the frequency step between the samples. They show that by increasing the observation bandwidth to 36–44 GHz, while keeping the number of samples constant (21), the decrease in the maximum imaging range can be noticed as the frequency step increases to 400 MHz. On the contrary, another simulation where the frequency step is decreased to 100 MHz while keeping 38–42 GHz bandwidth, shows that the maximum range can be increased. However, this increases the number of evaluated frequency points and thus raises the calculation time of the method.

Furthermore, the displacement of the target in each point has been recorded. The mean values of range and angle errors in pixels have been calculated for each simulation case using the same angle and range points so that the error results are comparable to each other. These results show that the range detection resolution becomes better as the bandwidth increases. The simulated results are collected to Table I.

The reconstructed image with five targets in 38–42 GHz bandwidth with 21 frequency samples is shown in Fig. 5. The results show that we can clearly locate multiple point targets in the space, though there can be a small error in range or angle component. However, these errors are very minor.

TABLE I
SIMULATED PERFORMANCE OF THE ESTIMATION METHOD

Bandwidth	Step	Max range	Angle error	Range error
38–42 GHz	200 MHz	139	2.070 points	1.699 points
36–44 GHz	400 MHz	74	1.907 points	0.984 points
38–42 GHz	100 MHz	>151	1.931 points	1.412 points

From these simulations can be deducted that where the range error is dependent on the used bandwidth and frequency step, the angle errors in imaging seem to be mostly related to the subarray radiation patterns. Still, the achieved angular resolution for imaging is quite good, when considering the wide width of the subarray beams and the small size of the total antenna array, the error is only some degrees.

IV. Conclusions

The imaging method for millimeter-waves has been presented and the performance of the method has been analyzed. The simulated results show that the targets can be identified quite well in the illuminated target space.

Future work includes prototyping the antenna and testing the method in practice. Furthermore, the image reconstruction method could be better optimized to achieve even faster image reconstruction.

References

[1] X. Gu, A. Valdes-Garcia, A. Natarajan, B. Sadhu, D. Liu, and S. K. Reynolds, "W-band scalable phased arrays for imaging and communications," *IEEE Communications Magazine*, vol. 53, no. 4, pp. 196–204, April 2015.

[2] P. Eudeline, "Survey of active electronically scanned antenna in Thales radars," in *2013 IEEE International Symposium on Phased Array Systems and Technology*, Oct 2013, pp. 12–16.

[3] A. K. Agrawal and E. L. Holzman, "Beamformer architectures for active phased-array radar antennas," *IEEE Transactions on Antennas and Propagation*, vol. 47, no. 3, pp. 432–442, March 1999.

[4] D. R. Jackson, C. Caloz, and T. Itoh, "Leaky-wave antennas," *Proceedings of the IEEE*, vol. 100, no. 7, pp. 2194–2206, July 2012.

[5] W. Menzel, "Planar leaky-wave antennas - early concepts and actual results," in *2013 European Microwave Conference*, Oct 2013, pp. 483–486.

[6] A. Basit, W. Khan, S. Khan, and I. M. Qureshi, "Development of frequency diverse array radar technology: a review," *IET Radar, Sonar Navigation*, vol. 12, no. 2, pp. 165–175, 2018.

[7] T. Fromenteze, C. Decroze, and D. Carsenat, "Waveform coding for passive multiplexing: Application to microwave imaging," *IEEE Transactions on Antennas and Propagation*, vol. 63, no. 2, pp. 593–600, Feb 2015.

[8] O. Yurduseven, T. Fromenteze, and D. R. Smith, "Relaxation of alignment errors and phase calibration in computational frequency-diverse imaging using phase retrieval," *IEEE Access*, vol. 6, pp. 14 884–14 894, 2018.

[9] J. Li and P. Stoica, "MIMO radar with colocated antennas," *IEEE Signal Processing Magazine*, vol. 24, no. 5, pp. 106–114, Sep. 2007.